Objectively combining AR5 instrumental period and paleoclimate climate sensitivity evidence

Supplemental Material

Nicholas Lewis[1]
Bath, United Kingdom

Peter Grünwald
CWI Amsterdam and Leiden University, the Netherlands

S1: Updating the Lewis and Curry (2015) final data year to 2015

Global temperature and changes ΔT therein

Lewis and Curry (2015; LC15) used HadCRUT4v2 for its GMST data. For the updated estimates, the latest version, HadCRUT4v4,[2] is used for calculation of all changes in GMST and of uncertainty therein. Doing so increases the TCR and ECS estimates based on the original 1995-2011 final period by 1.2%. The increase in mean GMST from the 1859–1882 base period to the updated 1995–2015 final period is 0.75 K.

Forcings and changes ΔF therein

All forcings used in LC15 were sourced from AR5 Table AII.1.2. These estimates are in principle of effective radiative forcing (ERF), but in practice are mainly based on estimates of stratospherically-adjusted radiative forcing (RF). In most cases, AR5 assessed there to be insufficient evidence for ERF differing from RF and took them to be the same. Only for anthropogenic aerosol forcing and the very small contrails/ contrail-induced cirrus forcing does the AR5 estimate ERF to differ from RF. In addition, AR5 estimated black carbon deposited on snow to have 2–4 times an effect on GMST per unit forcing, compared to other types of forcing. This was taken account of in the forcing values used in LC15. For volcanic forcing, it is not apparent that AR5 considered the relationship between RF and ERF.

---

[1] E-mail: nhlewis@btinternet.com

[2] http://www.metoffice.gov.uk/hadobs/hadcrut4/data/current/time_series/HadCRUT.4.4.0.0.annual_ns_avg.txt

Values for each individual forcing given in AR5 Table AII.1.2 were updated from 2011 to each of years 2012 to 2015 using observational data where available and otherwise whatever method was considered most appropriate, as follows.

Well mixed greenhouse gases

Forcing from CO_2, CH_4 and N_2O was calculated for each year from 2011 to 2015 using data for mean atmospheric concentrations,[3] and the formulae in AR5 8.SM (which imply a forcing of 3.71 Wm^{-2} for a doubling of CO_2 concentration). Forcing from minor GHGs was projected based on the recent growth rates and levels of forcing by CFCs, HCFCs and HFCs shown in AR5 Figure 8.6. We estimate that these imply a growth rate of 0.02 $Wm^{-2}decade^{-1}$, in line with the growth rate implied by the difference between the 2005 and 2011 'Total halogens' forcing values in AR5 Table 8.2. The annual change from 2011 in the thus calculated total forcing from GHGs was then added to the AR5 2011 GHG forcing estimate of 2.83 Wm^{-2} (which uses marginally different concentrations of CO_2, CH_4 and N_2O). This results in the 2015 GHG forcing value being 2.98 Wm^{-2}, of which CO_2 accounts for 1.94 Wm^{-2}.

Aerosols

AR5 estimates that total aerosol forcing declined at a rate of 0.24% per annum over 2002–11. Global aerosol optical depth (AOD) estimates over 2004–12 from three satellite instrumentation based datasets and a specialised model driven by assimilated meteorological observations are very similar, with three having trends indistinguishable from zero and one a trend of approximately −1% per annum, all with no sign of any change in trend (Ma and Yu 2015, Figure 1.a). Consistent with this, the AR5 estimates are extrapolated from −0.90 Wm^{-2} in 2011 to 2012–15 using the same −0.24% per annum trend as over 2002-11, reaching −0.891 Wm^{-2} in 2015.

Ozone

AR5 presents evidence for both tropospheric and stratospheric ozone concentrations gradually increasing since the late 20th century, resulting in positive forcing trends. We are not aware of any strong evidence that these trends have changed materially since 2011. Although satellite observations suggest that the post 2011 increase in stratospheric ozone

[3] Concentrations up to 2014 are from http://ds.data.jma.go.jp/gmd/wdcgg/pub/global/globalmean.html. The increase from 2014 to 2015 was based as follows: for CO_2, on the Mauna Loa mean from ftp://aftp.cmdl.noaa.gov/products/trends/co2/co2_annmean_mlo.txt; for CH_4, on the smoothed trend curve at http://www.esrl.noaa.gov/gmd/ccgg/trends_ch4/; and for N_2O on data at ftp://ftp.cmdl.noaa.gov/hats/n2o/combined/HATS_global_N2O.txt

forcing has been rather faster than per the trend over the previous decade,[4] the difference in forcing relative to the 2001–11 trend only reaches 0.005 W m^{-2} by 2015 and the data are noisy. Therefore, we extrapolate the AR5 2011 tropospheric and stratospheric ozone forcing values using their respective trends over the decade to 2011. The change in total ozone forcing by 2015 is an increase of 0.007 Wm^{-2}.

Other anthropogenic forcings

The AR5 estimates for minor land use change (albedo), stratospheric water vapour, black carbon on snow and contrails forcings have likewise been extrapolated from 2011 to 2015 using their trends over the decade to 2011. The net effect is an increase in forcing of 0.008 Wm^{-2} by 2015.

Solar

We updated solar forcing using TSI data from SORCE,[5] rebasing it to give the same anomaly, 0.03 Wm^{-2} , in 2011 as per AR5. Solar forcing climbs over 2012–15, reaching 0.093 Wm^{-2} in 2015.

Volcanic

The post 1850 AR5 volcanic forcing estimates are slightly rounded from −25x stratospheric AOD, based on the Sato dataset.[6] The latest value in that dataset is for 2012, and implies a slightly smaller forcing of −0.107 Wm^{-2} in 2012, very close to the AR5 2006–11 mean, than in 2011, which was more affected by the Nabro eruption. Sulphur dioxide emissions from explosive volcanic eruptions during 2013 to 2015 and the resulting stratospheric AOD levels remained at a similarly modest level to those in 2012 (Carn et al. 2016, Figure 9). We have therefore taken volcanic forcing to be −0.107 Wm^{-2} throughout 2012-15.

Total forcing

The estimated change in total forcing between 2011 and 2015 is 0.26 Wm^{-2}, of which 0.15 Wm^{-2} is due to increases in well-mixed (long lived) greenhouse gases (GHG) and 0.06 Wm^{-2} due to rising solar forcing, both of which are based on observational data. Changes in other

---

[4] KNMI MSR ozone data (downloaded using KNMI Climate Explorer [http://climexp.knmi.nl/] as Monthly observations field 'Ozone concentration *1978-now: KNMI multi-sensor re-analysis + sciamachy*', after conversion to global and annual mean data) shows a global increase of 4.2 Dobson units for 2015 over the mean for 2008-11, and regressing AR5 stratospheric O_3 forcing on the MSR data yields a slope of 0.0016 Wm^{-2} Dobson $unit^{-1}$ (correlation: 0.80), implying 2015 forcing of −0.043 Wm^{-2} vs −0.048 Wm^{-2} from continuing the 2001-11 trend.

[5] Downloaded from http://lasp.colorado.edu/lisird/sorce/sorce_tsi/index.html; divided by 4 to give mean TOA downward solar radiation

[6] http://data.giss.nasa.gov/modelforce/strataer/tau.line_2012.12.txt

forcings accounted for the remaining 0.05 Wm^{-2} of the increase. The increase in mean total forcing from the 1859–1882 base period to the updated 1995–2015 final period is 2.06 Wm^{-2}. Uncertainties are calculated from scaled 2011 AR5 estimates, exactly as in LC15.

Heat content and changes ΔQ in heat uptake

The planetary heat uptake rate, *Q*, is dominated by changes in ocean heat content (OHC). The 0-700 m layer OHC dataset (updated from Domingues et al 2008)[7] used in AR5 ends in 2011. Moreover, it is necessary to switch from 3 and 5 year averages, used in AR5 for the 0–700 m and 700–2000 m ocean layers, to annual means in order to be able to update beyond 2013. The NOAA (Levitus et al. 2012) OHC dataset,[8] used in AR5 for the 700–2000 m layer, is employed to provide changes over the full 0–2000 m layer from 2011 to each of the subsequent four years (taking changes in annual rather than pentadal mean global values for the final two years), obviating the need for a separate 0–700 m dataset. The minor deep (>2000 m) ocean, land and ice heat content amounts are updated from 2011 based on their trends over 2000–11. For the atmosphere, updating is based on the change in GMST since 2011 and the regression slope of heat content on GMST over 2000–11.

LC15, following Otto et al. (2013; Oa13), used the difference between the OHC estimates for the first and last years when calculating planetary heat uptake for the final period. With the final year OHC no longer representing an average over several years, it is much preferable to estimate heat uptake using the linear trend over the period rather than the differencing method. Based on the linear trend in OHC, the 1995–2015 heat uptake rate is 0.63 Wm^{-2}. As it happens, it is the same when calculated using the previous differencing method. Deducting the estimated 0.15 Wm^{-2} heat uptake rate over the 1859–1882 base period gives an increase of 0.48 Wm^{-2} in planetary heat uptake between the two periods.

Since error standard deviation estimates are available for all years of OHC data, uncertainty in the regression slope is estimated by performing a large ensemble of regressions each with all individual year heat content values perturbed by random draws from their uncertainty distributions. To allow for non-independence of errors in nearby years, which is to be expected even when 3 or 5 year running means are not used, all estimated heat content

[7] Data available at ftp://ftp.marine.csiro.au/pub/legresy/ohc/GOHC_recons_version3.0_1950_2011_CLIM_sbca12tmosme_OBS_bcax_0700m.dat

[8] Data available at http://www.nodc.noaa.gov/OC5/3M_HEAT_CONTENT/basin_avt_data.html

uncertainties are multiplied by sqrt(3). This multiplier reflects the dominance of uncertainty in 3-year mean 0–700 m OHC until the mid 2000s. Its use results in a slightly lower standard error estimate for the 1995–2011 heat uptake rate, of 0.082 Wm^{-2}, than the 0.087 Wm^{-2} when using the difference method. That is consistent with use of regression producing only a modest reduction in uncertainty for estimating heat uptake over fifteen years when the initial and final values used in the difference method are dominated by means over several years.

The scaled-down model-derived estimates of heat uptake in the base period, and uncertainty therein, are unchanged from LC15.

The thus estimated annual mean planetary heat uptake rate over 1995–2015, of 0.63 Wm^{-2}, is rather higher than the 0.51 Wm^{-2} over 1995-2011 used in LC15. If instead the Ishii and Kimoto (2009) 0–700 m dataset,[9] which has been updated to 2015, were used over the whole period, with the NOAA dataset continuing to be used just for the 700–2000 m layer after 2011, the linear trend planetary heat uptake estimate would be slightly lower at 0.57 Wm^{-2}, resulting in the main ECS estimate being 0.05°C lower. The heat uptake and ECS estimates would also be marginally lower if the NOAA dataset were used for the full 0–2000 m ocean layer over the whole period rather than just post 2011.

Estimation of ECS and the transient climate response (TCR)

ECS and TCR were estimated from the updated global temperature, forcing and heat uptake data in exactly the same way as for the original LC15 results.

S2: Using AOGCMs to estimate the relationship of ECS to $E_{ff}CS$

For AOGCMs, ECS is normally estimated (Andrews et al. 2012; AR5 Table 9.5) as half the *x*-intercept from a regression of top-of-atmosphere radiative imbalance (*N*) against change in GMST (*T*) as simulated over the 150 years following an abrupt quadrupling of atmospheric carbon dioxide (CO_2) concentration (abrupt4xCO2). For many AOGCMs, the local slope of a plot of *N* against *T* weakens during the 150 years (Andrews et al. 2015), resulting in a lower *x*-intercept if the regression is carried out over a shorter period. Nevertheless, the response in such models to a combination of arbitrary forcing series generally matches quite accurately the sum of its responses to the individual forcing series. The development of forcing during the instrumental

[9] Available at http://www.data.jma.go.jp/gmd/kaiyou/english/ohc/ohc_global_en.html

period approximates a 70-year linear ramp (Oa13 and LC15). At the end of a 70-year linear ramp the mean period over which a forcing increment has been applied is 35 years. Suppose that the response to the composite forcing over the instrumental period develops similarly to that for purely CO_2 forcing. On that basis, half the *x*-intercept from regressing *N* against *T* over the first 35 years of the abrupt4xCO2 simulation by an AOGCM provides an approximation to the estimate, $E_{ff}CS$, of ECS that would be derived from evidence available over the instrumental period, if the relevant characteristics of the real climate system matched those of that AOGCM. Accordingly, the ratio of the *x*-intercepts from regressing *N* against *T* over respectively 35 and 150 years of abrupt4xCO2 data provides an estimate of the ratio of $E_{ff}CS$ to ECS. Although this simple approach involves a number of assumptions, it is considered adequate for illustrating the sensitivity of the results to relaxing the assumption of constant feedback strength made in energy budget approaches. More sophisticated methods are outside the scope of the present study.

A ratio of $E_{ff}CS$ to ECS is calculated on the foregoing basis for each standard physics (p1) version AOGCM used in AR5 for which valid abrupt4xCO2 and preindustrial control run simulation data is available. In addition to the twenty three AOGCMs for which ECS estimates are shown Table 9.5 of AR5, six additional AOGCMs for which the requisite data is now available have been included, giving twenty nine models in all. Fitted values for *T* and *N* derived from linear regression over each model's full control run were deducted from its abrupt4xCO2 simulation annual mean *T* and *N* values, by reference to the period in the control run to which that simulation corresponded. Using pentadal means of the resulting adjusted values, *N* was regressed against *T* over both 35 and 150 years to obtain estimates of respectively $E_{ff}CS$ and ECS for each model, and their ratio calculated, with the results set out in Table S1.

Some of the assumptions involved in this simple approach can be explored. The approach implicitly assumes that instrumental-observation based estimation of $E_{ff}CS$ uses a measure of the effective radiative forcing (ERF) from a doubling of atmospheric CO_2 concentration ($F_{2\times CO2}$) consistent with that derived as half the *y*-intercept from a regression of *N* against *T* over the first 35 years of the abrupt4xCO2 simulation. Sensitivity to this assumption is fairly low, since in instrumental-observation based $E_{ff}CS$ estimation the same $F_{2\times CO2}$ value is normally used for CO_2 forcing as for converting climate feedback strength to $E_{ff}CS$ (Lewis 2015), but its validity is nevertheless of interest. A comparison of $F_{2\times CO2}$ estimated from fixed sea-surface temperature simulations, for eleven AOGCMs (Vial et al. 2013), with that estimated from regressions over the first 35 years of the abrupt4xCO2 simulations for the same models, shows that the two estimates

have almost identical means, and that they differ quite modestly for individual models. Moreover, results are very little changed when $E_{ff}CS$ values are calculated from 35 year regression slopes using a common, multimodel mean, 35-year regression derived $F_{2\times CO2}$ rather than using the individual model $F_{2\times CO2}$ values implicit in their regression *y*-intercepts. Doing so marginally increases the mean estimated $E_{ff}CS/ECS$ ratio but also increases its standard deviation, leaving the effect on combined-evidence estimation unchanged.

Sensitivity to the length of the regression that is used to estimate $E_{ff}CS$ corresponding to that derivable from evidence available over the instrumental period can also be examined. Regressing over 30, 25 or 20 years and/or using annual data, instead of regressing over 35 years using pentadal data, very marginally reduces the mean estimated model $E_{ff}CS/ECS$ ratio; the standard deviation increases modestly.

The assumption that the response to the composite forcing over the instrumental period develops similarly to that for purely CO_2 forcing is standard when estimating $E_{ff}CS$ from warming over the instrumental period. Hansen et al. (2005) provide evidence for the validity of this assumption; Lewis (2015) also provides some support for it. So does the fact that the Oa13 method, which does not depend on this "unit efficacy" assumption, generated a best-constrained (2000s data) TCR estimate with exactly the same median as the primary LC15 TCR estimate.

Too few AOGCMs have been run to equilibrium after a doubling of CO_2 concentration to assess the accuracy of the standard method of estimating their ECS from a 150 year regression of *T* against *N* following an abrupt quadrupling of CO_2 concentration. In most cases, regressing over years 21–150 rather than 1–150 produces a higher ECS estimate, but it is unclear whether that estimate is generally more accurate than one based on regressing over years 1–150.

A normal distribution with mean and standard deviation rounded to 0.925 and 0.065 respectively provides a reasonable fit to the data in Table S1, with three models having $E_{ff}CS/ECS$ ratios falling more than one standard deviation above the mean and four models having ratios falling more than one standard deviation below it. However, in order to make some allowance for non-normality and the additional uncertainties discussed in the exploration of assumptions, a substantially higher standard deviation, of 0.10, is adopted. An adjusted version of the RS93 posterior fit to the LC15 ECS distribution (which represents $E_{ff}CS$) is obtained by fitting a RS93 posterior to the histogram of the ratio of a large number of paired samples drawn from the original version of that fitted distribution and a N(0.925, 0.10) distribution.

Model	$E_{ff}CS$ / ECS
ACCESS1-0	0.830
ACCESS1-3	0.831
bcc-csm1-1	0.958
bcc-csm1-1-m	0.948
BNU-ESM	1.019
CanESM2	0.928
CCSM4	0.911
CNRM-CM5	1.036
CNRM-CM5-2	0.982
CSIRO-Mk3-6-0	0.760
FGOALS-g2	0.821
FGOALS-S2	0.940
GFDL-CM3	0.881
GFDL-ESM2G	0.971
GFDL-ESM2M	0.988
GISS-E2-H	0.950
GISS-E2-R	0.877
HadGEM2-ES	0.910
inmcm4	1.024
IPSL-CM5A-LR	0.978
IPSL-CM5A-MR	0.942
IPSL-CM5B-LR	0.910
MIROC-ESM	0.924
MIROC5	0.982
MPI-ESM-LR	0.917
MPI-ESM-MR	0.931
MPI-ESM-P	0.925
MRI-CGCM3	0.955
NorESM1	0.882
Mean	*0.928*
Standard deviation	*0.063*

Table S1. Ratio of effective climate sensitivity to equilibrium climate sensitivity estimates derived from the *x*-intercepts upon regressing *N* against *T* over respectively years 1–35 and years 1–150 of abrupt4xCO2 simulations by current generation AOGCMs.

S3: Changing the functional form of the distribution fitted to PDFs

The paper uses the RS93 posterior, ratio-normal approximation distribution as the primary functional form for the fitting of PDFs for ECS. Here, some additional results are presented based on the use of alternative functional forms, specifically the log-normal and the shifted log-*t* distributions. We first show that the LC15 pdf can also be well fitted by a shifted log-*t* distribution, but that the resulting inference from the combined (instrumental and paleo) evidence is then quite different between the objective Bayes and SRLR methods. This suggests that shifted log-*t* distributions are not as suitable as ratio-normal distributions here, consistent with the fact that the ratio-normal model is the physically more appropriate one. We then provide further insight into the discrepancy by considering the likelihoods that, on the basis of the objective Bayes method, underlie the posterior PDFs fitted to the original LC15 PDF; whereas that PDF is fit well both by the RS93 posterior approximation to a ratio-normal distribution and by a shifted log-*t* distribution, the likelihood corresponding (according to the SRLR method) to the LC15 PDF is only fit well by the ratio-normal likelihood.

A shifted lognormal distribution – one where the log of the variable plus a constant has a normal distribution – can be used to represent uncertainty with variable skewness (Meinshausen et al. 2009, there termed a skewed normal). As there are only three free parameters (the shift constant and the normal distribution mean and standard deviation), it can be fitted to the paleoclimate range and median, uniquely, as well as to the LC15 energy budget PDF. However, it provides a far poorer fit to the LC15 PDF than does a ratio-normal approximation, both visually and in terms of CDF percentage points. That is not surprising, since a ratio-normal distribution corresponds much more closely to the mathematical model of the physical problem that gave rise to the estimates of ECS. It is, however, possible to achieve a very good fit to the LC15 PDF over all but the extreme right hand tail of the distribution if a shifted log-*t* distribution is used (Lewis 2014). The replacement of the normal distribution by a scaled non-central *t*-distribution provides much more flexibility as to the shape of the distribution, at the expense of a fourth free parameter. In this case, the optimum *t*-distribution has just under 3.5 degrees of freedom, corresponding to a much fatter-tailed distribution than a normal. The Jeffreys prior for a shifted lognormal or log-*t* distribution is proportional to the reciprocal of the shifted variable and hence asymptotes to declining with ECS^{-1} at high ECS, compared with ECS^{-2} for a ratio-normal distribution. The fitted PDF matches the LC15 PDF well over most of its range despite the slower-declining prior

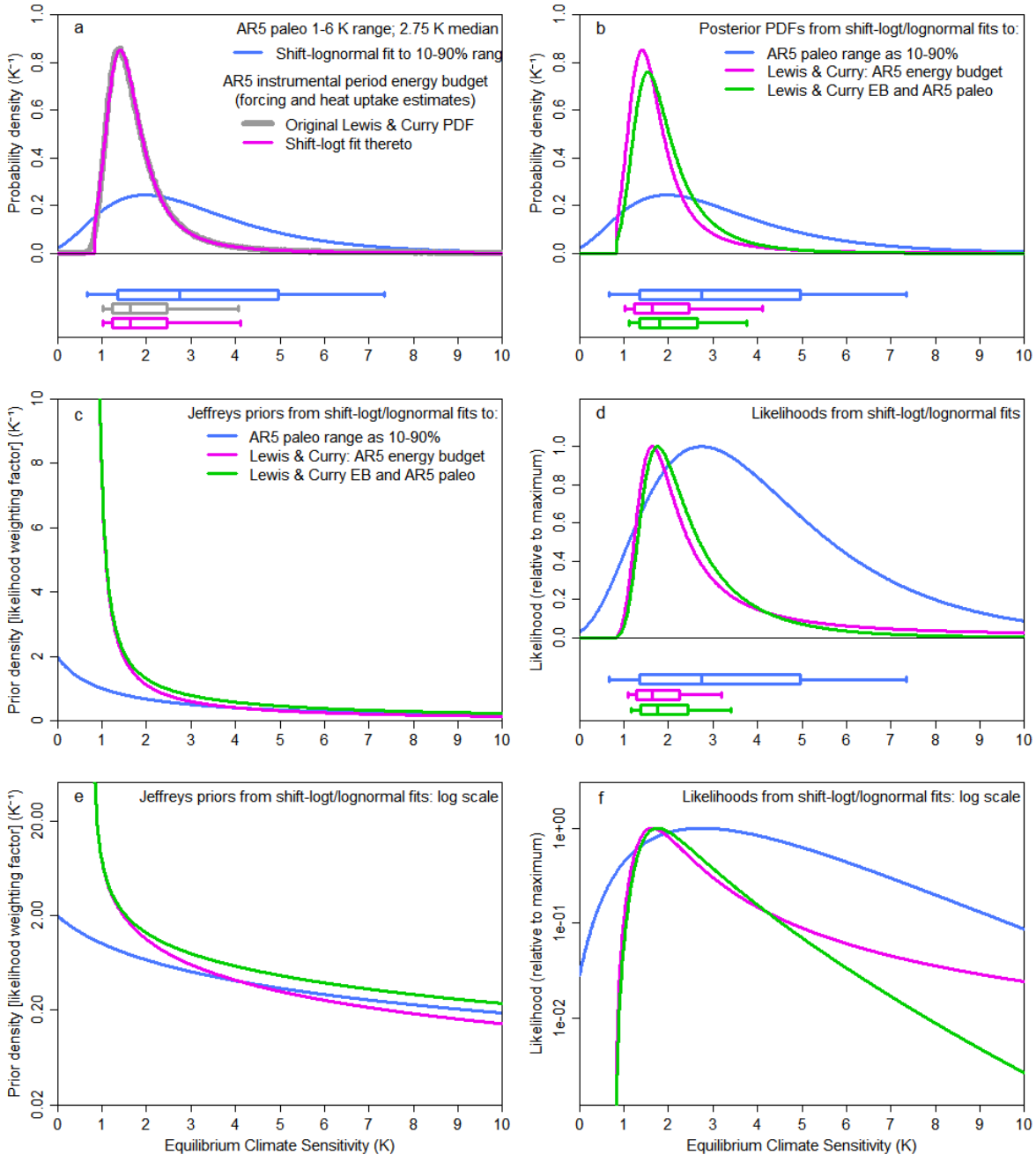

FIG. S1. Inference based on fitted PDFs for ECS using a shifted log-*t* distribution for evidence derived from the AR5 instrumental period forcing and heat uptake estimates using an energy budget approach (represented by the Lewis and Curry 2015 results) and shifted lognormal distributions for the AR5 paleoclimate 1–6 K range (taken as 10–90%) and 2.75 K median. The panels show: (a) the shifted log-*t* fit to the LC15 estimated PDF (magenta; original PDF in grey) and shifted lognormal fits to the AR5 paleoclimate range and median (blue); (b) posterior PDFs for the combined energy budget and paleoclimate evidence (green), being the normalized products of the corresponding likelihoods and Jeffreys priors, and, for comparison, the fitted posterior PDFs shown in (a); (c) the noninformative Jeffreys priors pertaining to each of the posterior PDFs in (b); (d) likelihood functions pertaining to each of the posterior PDFs in (b); (e) as for (c) but with a logarithmic *y*-axis scale; and (f) as for (d) but with a logarithmic *y*-axis having the same scale as in (e). The box plots indicate boundaries, to the nearest grid value, for the percentiles 5–95 (vertical bar at ends), 17-83 (box-ends), and 50 (vertical bar in box). The

box plots in panels (a) and (b) show Bayesian credible intervals calculated from posterior PDFs and allow for probability that lies outside the *x*-axis ECS range. The box plots in panel (d) show confidence intervals derived from the corresponding likelihood functions using the SRLR method.

because the shifted log-*t* likelihood function declines, beyond its peak, much faster with ECS than does the likelihood for a ratio-normal distribution. However, the fitted PDF's behavior in the extreme tails of the distribution, where it has a hard cut off at the lower end and declines more slowly than with ECS^{-2} at very high ECS values, does not accord with the characteristics of energy-budget based estimation.

Figure S1 shows the same information as Figure 3 regarding PDFs, likelihood functions and priors (omitting Oa13) but with fitting a shifted log-*t* distribution to the LC15 PDF and (as a range and median are insufficient to specify a shifted log-*t* distribution) a shifted lognormal for the paleoclimate estimate, rather than fitting RS93 posterior, ratio-normal approximation distributions to both. A shifted lognormal or log-*t* posterior distribution is easily factored into a likelihood function and a noninformative Jeffreys prior (by transforming the noninformative uniform prior applicable to the underlying normal or *t*-distribution). Jeffreys prior for inference from the combined evidence is obtained by adding the two separate Jeffreys priors in quadrature, and is multiplied by the product of the likelihood functions to obtain the posterior PDF, as in the ratio-normal approximation case. ECS percentage points derived from the combined-evidence PDFs (Figure S1(b)) are similar to those based on ratio-normal approximation fits, but with their medians closer to that for the LC15 energy budget study and somewhat lower 83% and 95% points than when using ratio-normal fits. Inference based directly on the likelihoods using the SRLR method (Figure S1(d)) agrees exactly for the fits to the paleoclimate range, since the SRLR method provides exact confidence intervals for any transformed normal distribution. However, the SRLR-based confidence intervals for the shifted log-*t* fit to the LC15 PDF are significantly narrower than the credible intervals derived from the fitted PDF, particularly as regards their upper percentage points. The differences between the combined-evidence estimates based on fitting ratio-normal and shifted log-*t* /lognormal PDFs almost entirely emanates from the different fit to the LC15 PDF. Swapping the fits to the paleoclimate range and median between ratio-normal approximation and shifted lognormal has little effect.

The differences in combined-evidence inference resulting from the use of alternative standard form distributions, both of which produce an excellent visual fit to the LC15 PDF used to represent instrumental period evidence, shows that it is important to consider not only the

characteristics of the data uncertainties for the physical quantities which underpin estimation of the parameter of interest, ECS, but also the mathematical physics of how that parameter is related to those physical quantities. A ratio of two normal distributions is much more closely related to what is involved in estimating ECS using an energy budget method, and gives rise to more appropriate behavior in the extreme tails of the distribution, than a low degrees of freedom shifted log-*t* distribution. This physically-based argument is supported by a comparison of the likelihood functions derived (using the relevant noninformative priors) from each of the two types of distribution fitted to the LC15 PDF for ECS, with an approximate likelihood derived directly from the original LC15 estimated PDF. The direct derivation consists of applying the SRLR method in reverse to obtain likelihood values from CDF values treated as confidence points. Figure S2 shows that the match is much closer for the ratio-normal fitted PDF than for the shifted log-*t* one.

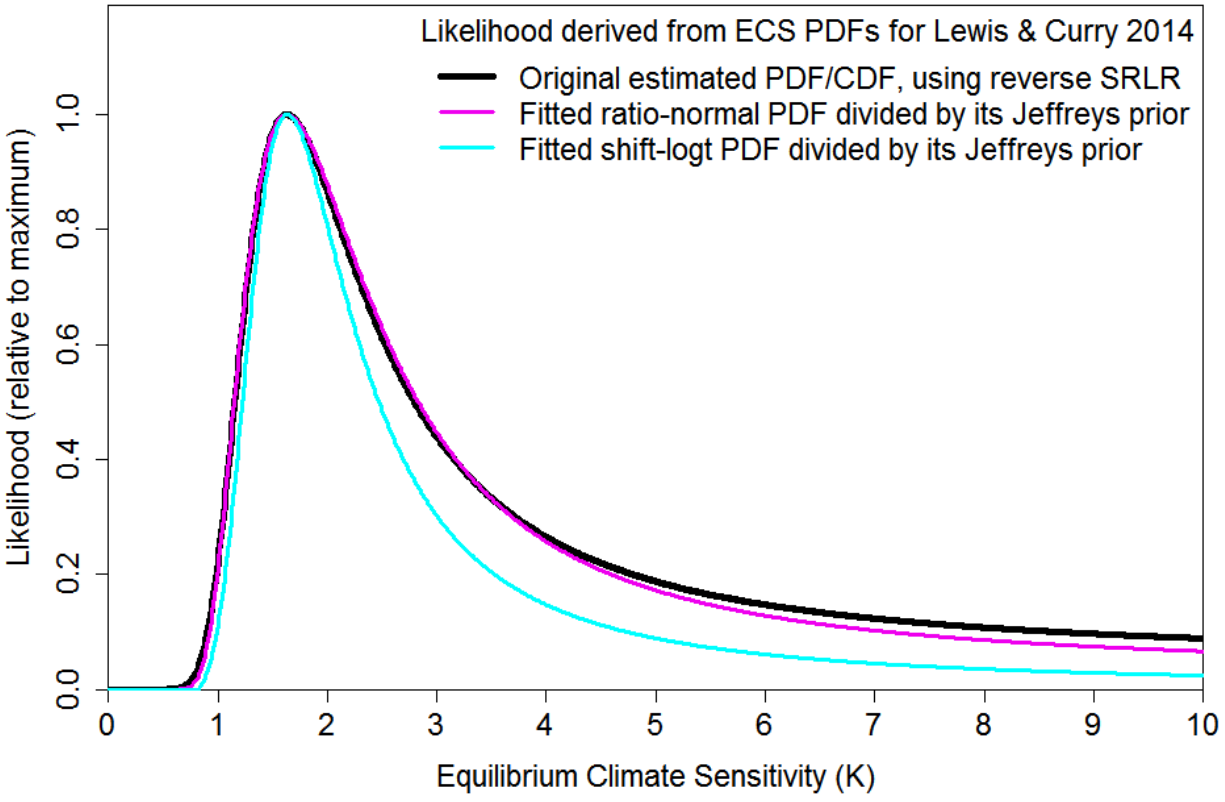

FIG. S2. Comparison of likelihoods derived from the PDF fitted to the Lewis & Curry 2015 AR5 instrumental period energy budget based estimated PDF for ECS using ratio-normal (magenta line) and shifted log-*t* (cyan line) distributions, by dividing them by the noninformative Jeffreys prior computed for the relevant fitted distribution, with an estimated likelihood derived from the original LC15 PDF by treating the corresponding CDF as a confidence distribution and applying the SRLR method in reverse (black line).

Additional references

Andrews, T., J. M. Gregory, M. J. Webb, and K. E. Taylor, 2012: Forcing, feedbacks and climate sensitivity in CMIP5 coupled atmosphere-ocean climate models. *Geophys. Res. Lett*., **39**, L09712

Andrews, T., J. M. Gregory and M. J. Webb, 2015._The dependence of radiative forcing and feedback on evolving patterns of surface temperature change in climate models. *J Clim*, **28**, 1630–1648

Carn S.A., L. Clarisse, A.J. Prata, 2016. Multi-decadal satellite measurements of global volcanic degassing. *Jnl of Volcanology and Geothermal Research* **311**, 99–134

Domingues, C.M., et. al., 2008. Improved estimates of upper-ocean warming and multi-decadal sea-level rise. *Nature,* **453**, 1090–3

Hansen J. et al., 2005. Efficacy of climate forcings. *J Geophys Res*, **110**: D18104, doi:101029/2005JD005776

Ishii M., Kimoto M., 2009. Reevaluation of historical ocean heat content variations with time-varying XBT and MBT depth bias corrections. *J Oceanogr,* **65**, 287-299

Lewis, N., 2015. Implications of recent multimodel attribution studies for climate sensitivity. *Clim Dyn*, DOI 10.1007/s00382-015-2653-7

Levitus S. et al., 2012. World ocean heat content and thermosteric sea level change (0-2000m) 1955-2010. *Geophys Res Lett* 39:L10603

Lindley, D. V., 1958, Fiducial Distributions and Bayes' Theorem. *J. Roy. Stat. Soc*, **20**, 102-7

Ma, X. and Yu, F., 2015. Seasonal and spatial variations of global aerosol optical depth: multi-year modelling with GEOS-Chem-APM and comparisons with multiple-platform observations. *Tellus B*, **67**, 25115

Meinshausen, M., et al., 2009: Greenhouse-gas emission targets for limiting global warming to 2 K. *Nature*, **458**, 1158–1162

Vial, J., Dufresne, J-L., Bony, S., 2013. On the interpretation of inter-model spread in CMIP5 climate sensitivity estimates. *Clim. Dyn.*, **41**, 3339-62